Soils and Rocks
An International Journal of Geotechnical and Geoenvironmental Engineering
www.soilsandrocks.com
ISSN 1980-9743
ISSN-e 2675-5475

A multivariable investigation of the critical state line in iron mine tailings

Leonardo Alberto do Nascimento[1#], Magnos Baroni[1], Dêreck Hummel Becher[1], Fernando Schnaid[2]

Article

Keywords
Tailings
Flow liquefaction
Critical state line
Index properties
Statistical analysis

Abstract

The geotechnical behavior of non-plastic tailings is governed by a unique critical state line (CSL) that, unlike those of many natural soils, may exhibit pronounced non-linearity associated with state transitions from strain-softening at low mean effective stresses to strain-hardening at higher stress levels. This study investigates the material properties and state variables controlling this behavior, with particular emphasis on their correlation with index properties and their role in defining inflection points associated with transitions from flow instability and liquefaction to stable soil response. A data-driven meta-analysis is performed using a global database of laboratory test results on iron tailings. The methodology integrates statistical characterization of physical attributes, followed by exploratory analysis using Spearman correlation matrices to identify the variables governing the shape and position of the CSL. Results demonstrate that CSL parameters are primarily controlled by minimum and maximum void ratios and specific gravity, while fines content and mineralogy exert secondary influences. The established correlations enable prediction of the CSL geometry, providing a practical screening framework for preliminary assessment of the geomechanical behavior of iron tailings and their susceptibility to liquefaction.

1. Introduction

The fundamental aspects of the geomechanical behavior of tailings can be effectively interpreted within the framework of Critical State Soil Mechanics (CSSM). Experimental evidence indicates that tailings tend to converge toward a unique Critical State Line (CSL), which is independent of initial density, fabric anisotropy, and stress path (e.g. Been et al., 1991; Delgado et al., 2025; Fanni et al., 2024; Salvatore et al., 2017; Schnaid et al., 2013). The Critical State is defined in the p'-q-e space (Schofield & Wroth, 1968) and its projection onto the q-p' plane corresponds to a linear strength envelope where:

$$q = M \cdot p' \tag{1}$$

where M is the critical stress ratio, directly related to the critical state friction angle Φ_{cs}.

Conventional CSL idealization in the $e - \log p'$ plot is assumed to be semi-log linear, expressed as:

$$e_c = \Gamma - \lambda_e \cdot ln\left(p_c'\right) \tag{2}$$

In this expression, e_c is the critical void ratio, Γ is the void ratio at the critical state at reference pressure of 1 kPa, p' is the mean effective stress, and λ_e is the slope of the CSL in a semi-logarithm plane (e - log p').

However, a notable characteristic of tailings is that the CSL frequently exhibits pronounced curvature, reflecting transitions between different mechanical states (Bedin, 2010; Been et al., 1991; Carrera et al., 2011; Schnaid et al., 2013; Verdugo & Ishihara, 1996). Such curvature can be described by a power-law relationship of the form:

$$e_c = a + b \cdot \left(\frac{p_c'}{p_{ref}'}\right)^c \tag{3}$$

here, a, b, and c are fitting parameters calibrated against experimental data, and p'_{ref} is taken as 1 atm (101.32 kPa).

Within this representation, the CSL tends to flatten at low mean effective stresses. This behavior is associated with a continuous reduction in undrained shear strength, ultimately leading to true liquefaction under sufficiently low confinement.

#Corresponding author. E-mail address: leonardo.alberto@acad.ufsm.br
[1]Universidade Federal de Santa Maria, Departamento de Transportes, Santa Maria, RS, Brasil.
[2]Universidade Federal do Rio Grande do Sul, Departamento de Engenharia Civil, Porto Alegre, RS, Brasil.

Submitted on May 18, 2026; Final Acceptance on September 23, 2026; Discussion open until February 28, 2027.
Editor: Renato P. Cunha
https://doi.org/10.28927/SR.2026.008926

This is an Open Access article distributed under the terms of the Creative Commons Attribution license (https://creativecommons.org/licenses/by/4.0/), which permits unrestricted use, distribution, and reproduction in any medium, provided the original work is properly cited.

Under such conditions, tailings are unable to sustain a constant deviatoric stress, exhibiting pronounced strain softening and failure by flow liquefaction. As the mean effective stress increases, the mechanical response evolves; although strain softening and high compressibility may still occur, the behavior progressively transitions toward strain hardening. At higher stress levels, the curvature of the CSL is commonly attributed to the onset of particle breakage (Bedin et al., 2012; Konrad, 2001; Lade, 1992; Schnaid et al., 2013).

Figure 1 illustrates the conceptual framework comparing linear and non-linear CSLs. The linear CSL is defined at intermediate stresses, beyond the non-linear CSL's horizontal asymptote and prior to pronounced curvature from particle breakage at higher confinement.

Relevant critical state parameters include: (i) linear CSL slope (λ) and intercept (Γ_L); and (ii) non-linear CSL parameters Γ_{NL}, a, b, and c. Two additional inflection points (e_{inst}, e_{sta}) evaluate the frameworks' interaction. Materials with void ratios above Γ_{NL} are highly susceptible to flow liquefaction. The domain between Γ_{NL} and the first intersection of the linear and non-linear CSLs (e_{inst}, p'_{inst}) defines an unstable region prone to flow instability.

A second intersection (p'_{sta}, e_{sta}) marks the onset of a stiffer CSL response governed by particle breakage. Within the interval bounded by these inflection points ($e \in [e_{inst}, e_{sta}]$ and $p' \in [p'_{inst}, p'_{sta}]$), the material exhibits a stable undrained shear response, and both CSLs effectively coincide.

These parameters govern the mechanical response of tailings and their susceptibility to static liquefaction. For preliminary design and risk assessment of tailings storage facilities (TSFs), correlating critical state parameters with index properties provides a valuable screening tool, bridging the gap between advanced laboratory characterization and routine testing.

While understanding of non-plastic mechanical behavior originates largely from sands (Jefferies & Been, 2016; Rabbi et al., 2019; Sadrekarimi, 2014), studies on mine tailings remain sparse (Almeida et al., 2025; Macedo & Petalas, 2019; Smith et al., 2019; Torres-Cruz & Santamarina, 2020). Literature consistently shows the CSL intercept (Γ_L) strongly correlates with extreme void ratios (e_{max} and e_{min}), acting as reliable proxies for the CSL position, whereas the void ratio range (e_{max} - e_{min}) governs compressibility (Jefferies & Been, 2016; Torres-Cruz & Santamarina, 2020).

Estimating the CSL slope (λ_e) is less accurate, as it depends on combined effects of *FC*, plasticity, and mineralogy. Although λ_e generally increases with fines and plasticity (Macedo & Petalas, 2019; Smith et al., 2019), *FC* alone is an unreliable predictor. Compressibility is better captured using combined grading and mineralogical descriptors (Ccotohuanca & Klassen, 2024; Macedo & Petalas, 2019; Smith et al., 2019), with harder siliceous minerals generally exhibiting lower λ_e values.

In contrast, parameter *M* is relatively insensitive to index properties. However, due to particle shape, surface texture, and mineralogy, tailings generally exhibit higher *M* values than natural sands (Macedo & Petalas, 2019; Torres-Cruz & Santamarina, 2020; Vick, 1990).

These trends support using index properties as practical proxies for critical state behavior. While triaxial testing remains the standard to define the critical state locus (e.g. Fonseca, 2026; Fonseca et al., 2021), this paper interprets triaxial data through a multivariable analysis of the CSL in non-plastic iron ore tailings (IOT). Because these inert materials lack clay minerals, diagenesis is generally negligible, with behavior governed primarily by particle size and shape (Mitchell, 1976; Mitchell & Soga, 2005). Although typically normally consolidated, microstructural features like aging or cementation may still locally modify their response.

2. Materials and methods

2.1 Database compilation and data processing

A global database of 49 experimental datasets from 23 studies was compiled, requiring physical characterization, testing procedures, and critical state parameters from laboratory triaxial testing. These predominantly non-plastic iron ore tailings cover a broad *FC* range (17%–99%).

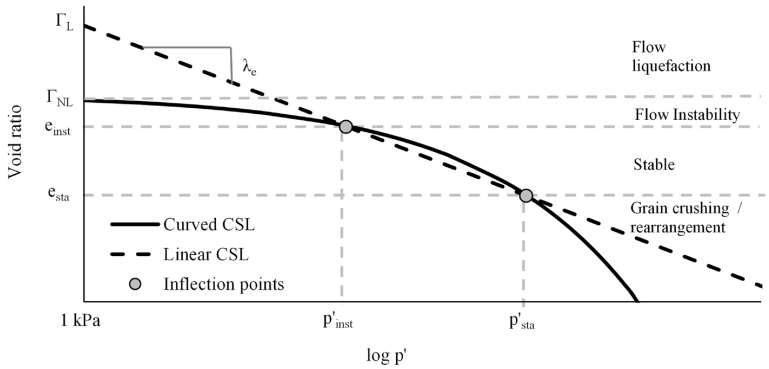


Figure 1. Illustration of linear and non-linear CSL and the corresponding parameters.

CC BY

The database and corresponding references are presented in Appendix A (Nascimento et al., 2026) compiled from Carneiro (2021), Carvalho et al. (2024), Ccotohuanca & Klassen (2024), Cella & Padovani (2021), Consoli et al. (2024a, 2024b), Delgado et al. (2023, 2025), Freire (2022), Gonçalves et al. (2025), Ji et al. (2024), Li & Coop (2019), Morgenstern et al. (2016), de Nóbrega (2021), Oliveira (2022), Reid & Fanni (2022), Reid et al. (2018), Rios et al. (2025), Robertson et al. (2019), Silva et al. (2022, 2024), and Wagner et al. (2023)

To ensure consistency, reported parameters were interpreted following ASTM standards for particle size distribution - ASTM D7928 (ASTM, 2021) -, specific gravity - ASTM D854 (ASTM, 2023) -, Atterberg limits - ASTM D4318 (ASTM, 2017) -, and extreme void ratios - ASTM D4254 (ASTM, 2016b) and ASTM D4253 (ASTM, 2016a). However, standardized procedures for determining minimum void ratio are inconsistently applied across published studies, and their suitability for fine-grained tailings remains questionable.

Extracted data included origin, disposal method, physical and mineralogical properties, and critical state parameters. Missing values were digitized from published figures, and parameter M was derived from the p'-q plane.

Both linear and non-linear CSL formulations were considered. For originally non-linear datasets, equivalent linear parameters were derived via least-squares regression at intermediate stresses. Conversely, estimating non-linear coefficients for datasets reporting only linear CSLs was avoided to prevent excessive subjectivity.

2.2 Statistical analysis

An initial data quality assessment removed physically implausible values to ensure reliability, followed by descriptive statistical analyses. Potential outliers were retained rather than excluded, as they represent the intrinsic variability of IOT - reflecting differences in mineralogical origin, beneficiation, deposition, and testing methods - ensuring a representative dataset.

Due to non-normal distributions, Spearman's rank correlation was adopted to evaluate monotonic relationships between variables. These correlations were compared with literature trends to identify consistencies and discrepancies. Strong correlations supported preliminary interpretations of CSL behavior based on fundamental parameters, though results were interpreted cautiously considering stress range, morphology, and fabric effects. Given the database heterogeneity, these relationships represent first-order trends rather than deterministic predictive laws.

Finally, multiple linear regression (MLR) using predictors from the Spearman matrix and bivariate relationships established a preliminary framework to predict critical state behavior in the e - log p' plane solely from fundamental characterization parameters.

3. Analysis and results

The analysis was divided into two parts, considering univariate and bivariate descriptive statistics.

3.1 Univariate descriptive statistics

Disposal methods are relatively balanced between hydraulically deposited (37%) and dewatered (33%) tailings, with 30% unreported. The predominance of Brazilian (86%) and Chinese (10%) tailings reflects these countries' major roles in global iron ore production (Almeida et al., 2025; IBRAM, 2025). Moist tamping predominated specimen preparation. Most studies used triaxial compression (72% drained and undrained), but 47% relied solely on isotropic consolidation, potentially failing to capture anisotropic field stresses.

Table 1 summarizes the dataset's descriptive statistics, with the Shapiro-Wilk test confirming non-normal distributions for most parameters.

The database includes fine-grained silts to sand-like tailings. As indicated by C_u and C_c values (Lambe & Whitman, 1979), these materials are generally well-graded, although a few poorly graded exceptions exist. As shown in Table 1, specific gravity considerably exceeds typical natural soils due to elevated iron oxide concentrations, while silicates remain the dominant mineral phase. This mineralogical variability - stemming from different sources and processing routes - significantly influences mechanical behavior. Finally, the analyzed tailings are predominantly non-plastic.

As detailed in Table 1, critical state parameters exhibit considerable variability. Notably, Γ_{NL} is consistently lower than Γ_L, emphasizing the need to capture low-stress curvature effects. For subsequent correlation analyses, mineralogy was excluded due to data scarcity; instead, the physical skeleton was characterized by D_{50}, C_u, FC, extreme void ratios, and G_s. Furthermore, Γ_{NL} and Φ_{cs} were excluded from correlation matrices due to conceptual redundancy with parameters a and M.

3.2 Bivariate descriptive statistics

The parameters selected for the univariate analysis were subsequently used to construct a Spearman correlation matrix, enabling the evaluation of pairwise relationships and the identification of positive and negative monotonic associations. The resulting correlation matrix for the complete dataset is presented in Figure 2.

Overall, the correlation matrix reveals relatively few strong relationships, suggesting that the mechanical behavior of IOT is governed by multiple interacting factors rather than by a single controlling variable.

The stress ratio parameter M exhibits weak correlations with most variables. Figure 3a compares the compiled database with literature data regarding the influence of FC in M.

CC BY

Table 1. Summary of univariate quantitative parameters analysis.

Parameter	Min.	Avg.	Max.	Std.	Med.	Samples	Normality
D_{10} (μm)	1	20	50	15	17	41	No
D_{30} (μm)	3	48	140	26	50	40	No
D_{50} (μm)	13	73	220	38	72	49	No
D_{60} (μm)	8	97	280	51	100	40	No
C_u	2	8	27	6	7	40	No
C_c	0	2	5	1	1	40	No
Clay (diameter < 0.002 mm)	0	4	23	4	3	40	No
Silt (0.002 mm < diameter < 0.075 mm)	17	49	90	19	46	40	No
Sand (0.075 mm < diameter < 4.75 mm)	1	43	83	22	48	50	No
G_s	2.7	3.5	5.0	0.7	3.2	50	No
Tested e_{min}	0.36	0.53	1.12	0.16	0.51	28	No
Tested e_{max}	0.85	1.16	1.37	0.15	1.20	28	Yes
WL	-	4	27	9	0*	48	No
WP	-	2	17	5	0*	48	No
PI	NP	1	14	3	0*	48	No
Silicates (%)	2.2	60.1	98.3	31.3	76.9	28	No
Aluminum oxides (%)	0.0	0.0	0.7	0.2	0*	28	No
Titanium oxides (%)	0.0	0.7	6.4	1.7	0*	28	No
Calcium oxides (%)	0.0	0.0	0.0	0.0	0*	28	No
Iron oxides (%)	0.0	31.8	95.2	27.8	20.9	28	No
Sulfides (%)	0.0	0.0	0.6	0.1	0*	28	No
Carbonates and halides (%)	0.0	0.0	0.3	0.1	0*	28	No
σ_{3max}	400	-	120000	-	1600	41	No
Molding moisture	6	12	15	2	13	16	Yes
Molding void ratio	0.53	0.81	1.25	0.18	0.75	31	No
Γ_L	0.795	1.053	1.640	0.176	1.020	40	No
λ_e	0.025	0.050	0.110	0.020	0.045	40	No
a	0.74	0.88	1.13	0.11	0.87	39	No
b	0.00	0.08	0.24	0.06	0.06	39	No
c	0.17	0.42	0.88	0.15	0.37	39	No
M**	1.32	1.36	1.40	0.04	1.36	39	Yes
Φ (º)	29.8	33.8	38.7	1.5	33.4	50	Yes
$p'_{inst.}$	30	174	500	142	100	31	No
$e_{inst.}$	0.64	0.81	1.06	0.12	0.79	31	No
$p'_{sta.}$	300	1294	4000	943	1000	31	No
$e_{sta.}$	0.52	0.72	1.00	0.14	0.70	31	No

*A median of zero indicates that the respective mineral group is absent in the majority of the compiled tailings. **Not considering axial extension test.
Legend: see List of Symbols.

Although Hussien & Sgaoula (2023) reported a moderate correlation between parameter M and FC, the observed variation remains relatively limited, with M mainly ranging from 1.29 to 1.42 across a fines content ranging from 0 to 100%.

Torres-Cruz & Santamarina (2020) argue that particle shape (specifically angularity) is the fundamental driver of frictional strength at the critical state, overriding the influence of particle size, mineralogy, or fines content. These authors reported a representative value of 1.34, which is consistent with the mean value of 1.37 reported by Ccotohuanca & Klassen (2024). This perspective is more consistent with the analyzed data and is supported by other authors (Bouckovalas et al., 2003; Freire, 2022; Li, 2013).

Regarding the extreme void ratios and their correlation with FC as shown in Figure 3b, Torres-Cruz & Santamarina (2020) indicate distinct patterns of behavior. Both e_{max} and e_{min}, exhibit a "U" shape correlation relative to FC, where the highest void ratios occur at extreme gradations, such as very low or very high fines contents. Conversely, the lowest values are observed at intermediate fines contents, typically between 30% and 60%, which corresponds to the densest granular packing (Li, 2017; Torres-Cruz, 2016).

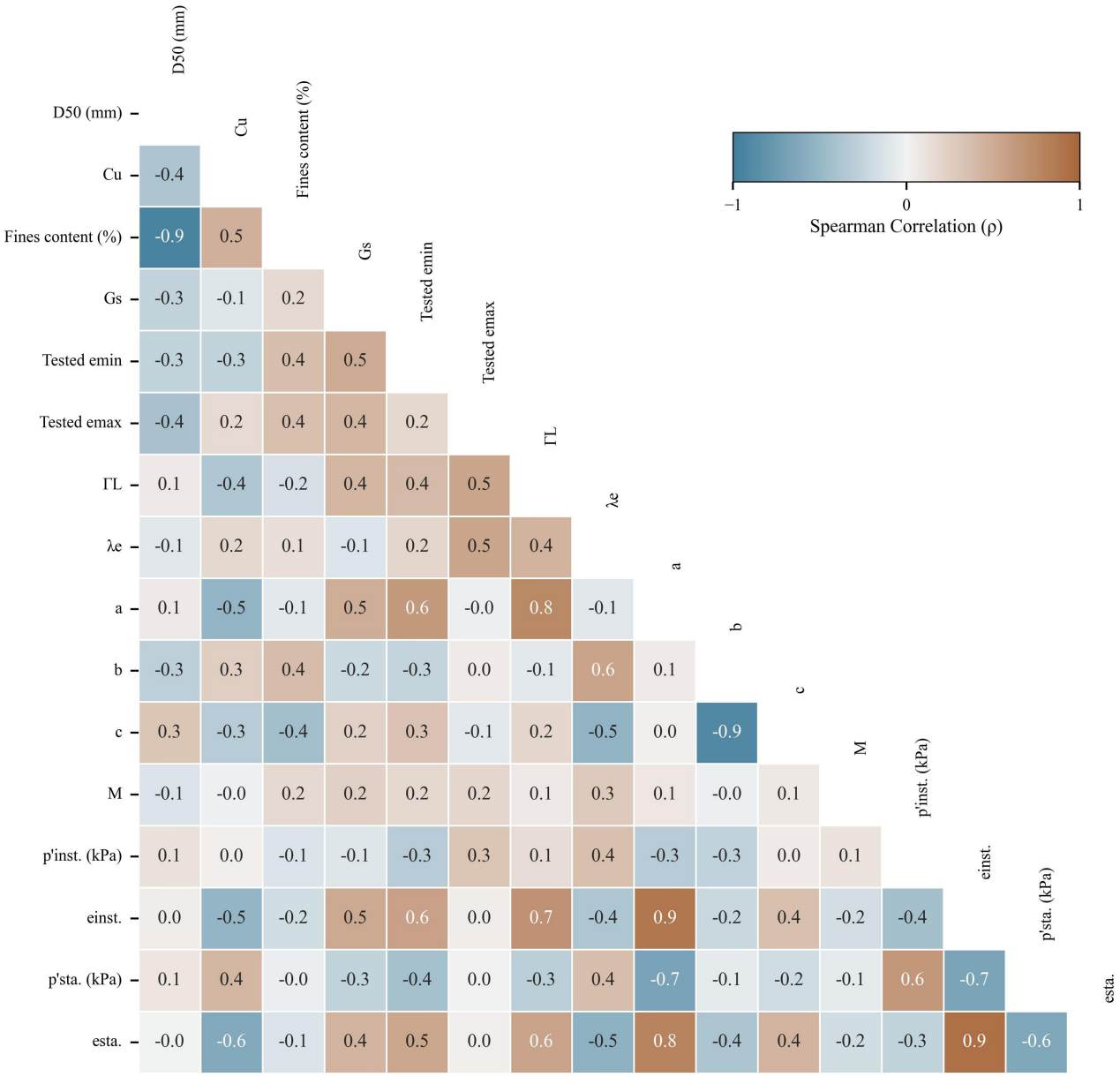


Figure 2. Spearman Matrix for parameters correlation.

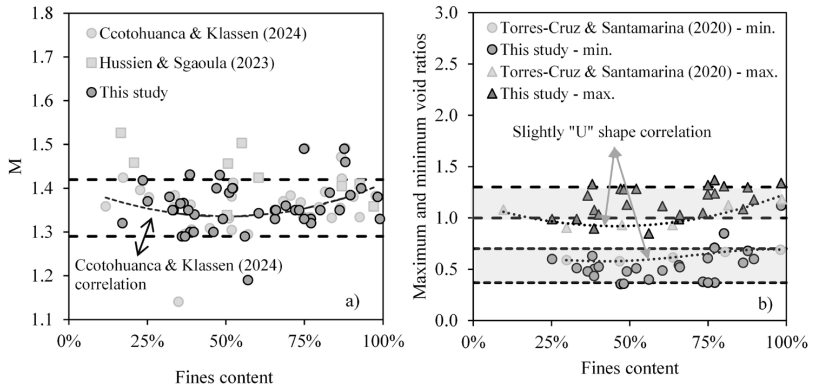


Figure 3. Relationship between the fines content and a) critical state stress ratio (*M*) and b) maximum and minimum void ratios.

The same trends can be noted in the iron database of this study. This specific proportion is widely recognized in the literature as the Threshold Fines Content or Transitional Fines Content (TFC), marking the critical point where fine particles transition from merely filling the interstitial voids to actively dominating the load-bearing matrix (Carrera et al., 2011; Li, 2017; Thevanayagam et al., 2002).

3.3 Critical State Line analysis and parameters correlations

Figure 4 presents both the linear and non-linear CSL formulations, illustrating the distribution of stable and unstable states specifically along the non-linear envelopes. The lower panels (Figure 4c and Figure 4d) present a normalized void ratio plane (e_{cs} / e_{cs0}), aiming to reduce data dispersion and highlight common behavioral trends between different materials.

Figure 4 is used to define stress ranges associated with the inflection points that characterize the material's susceptibility domains. The instability zone is concentrated at low mean effective stresses (50–150 kPa), whereas the stability zone predominates at higher stress levels (500–1500 kPa). Furthermore, as the mean effective stresses that characterize the instability and stability points increase, the corresponding voids ratios decrease, a trend that is confirmed by the Spearman Matrix Correlation.

3.3.1 Linear CSL

Figure 5 compares the correlation of linear CSL parameters and *FC* obtained from the compiled database. As previously mentioned, λ_e and Γ_L were obtained from datasets originally reported with non-linear CSLs adjusted via least-squares regression. They do not necessarily represent the material behaviour at critical state, especially at the low stress range.

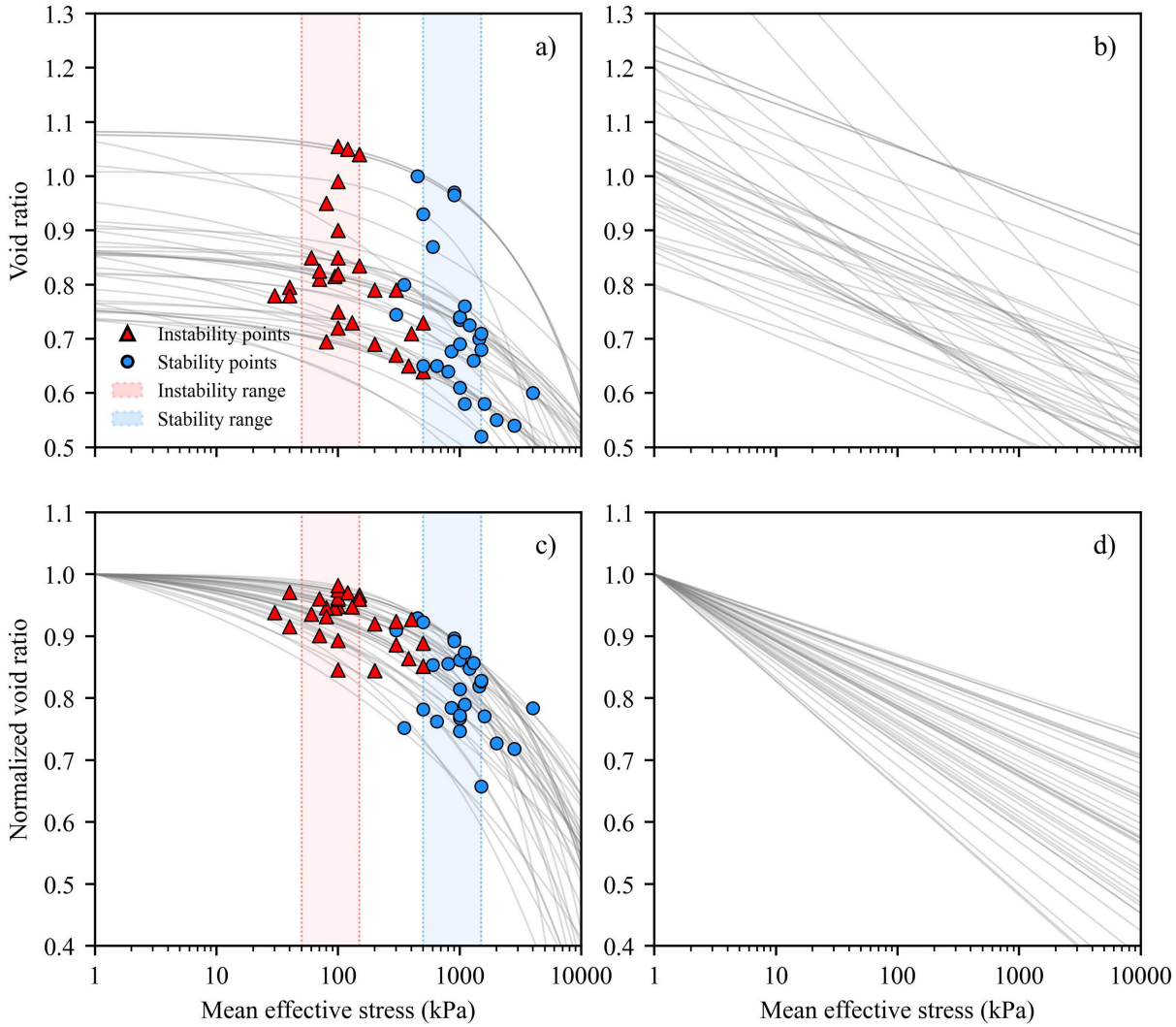


Figure 4. Critical State Lines from analyzed dataset separated in a) non-linear CSL; b) linear CSL; c) normalized non-linear CSL and d) normalized linear CSL.

As illustrated earlier in Figure 2, *FC* does not exert a significant direct influence on the linear CSL parameters, an empirical observation that is well supported by previously published data (Ccotohuanca & Klassen, 2024; Jefferies & Been, 2016; Macedo & Vergaray, 2022; Reid, 2015; Smith et al., 2019; Torres-Cruz, 2016). However, the "U" shape correlations previously identified by Torres-Cruz & Santamarina (2020) are also present in Figure 5, suggesting a correlation between these parameters (λ_e and Γ_L) and extreme void ratios, detailed in Figure 6.

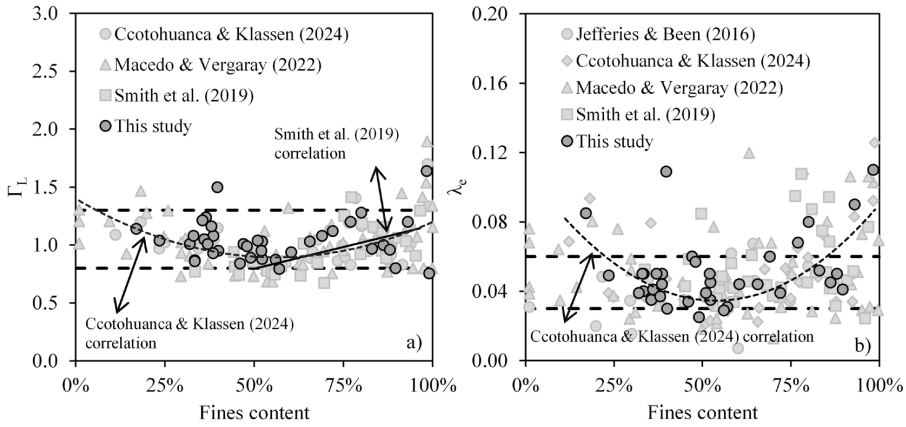


Figure 5. Relationship between fines content and linear CSL parameters a) Γ_L and b) λ_e.

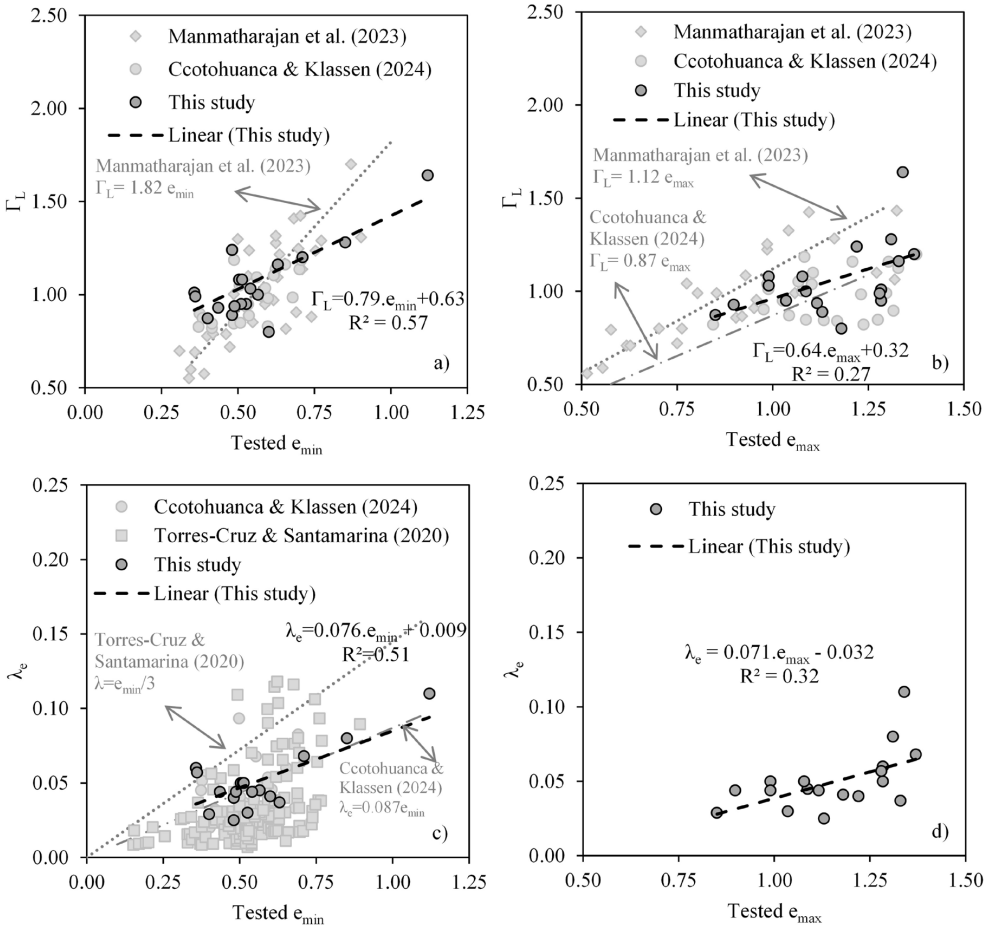


Figure 6. Correlation between minimum and maximum void ratio and linear CSL parameters: *a* and b) Γ_L and *c* and d) λ_e.

CC BY

From a micromechanical perspective, the observed "U" shape correlation pattern can be attributed to the void-filling mechanisms associated with the fines fraction. At fines contents below 50%, the material is structurally dominated by a skeleton of sand-sized particles, while fine particles primarily occupy intergranular voids (Smith et al., 2019). As fines content approaches intermediate values, the fines fraction progressively integrates into the load-bearing skeleton, promoting denser packing arrangements and reducing material compressibility. This behavior is reflected by lower values of both λ_e and Γ_L parameters. However, when fines content exceeds approximately 50%, the nature of the particle contacts undergoes a transition and becomes predominantly controlled by a matrix of silt and clay-sized fines, returning to the TFC concept (Carrera et al., 2011; Li, 2017; Thevanayagam et al., 2002). This shift in the structural skeleton reverses the packing behavior, thereby increasing the overall compressibility of the material (Ccotohuanca & Klassen, 2024; Smith et al., 2019).

In contrast to *FC*, more pronounced relationships are observed between linear CSL parameters and the extreme void ratios, as illustrated in Figure 6. This highlights the dominant role of packing characteristics in controlling critical state behavior. In general, the linear CSL parameters exhibit positive correlations with both minimum and maximum void ratios. Stronger relationships are observed for e_{min}.

The apparent discrepancy between the Spearman correlation matrix and the regression trends shown in Figure 6 is statistically consistent, as both approaches capture distinct aspects of the dataset. The Spearman's rank correlation coefficient is based on ordinal ranking and identifies monotonic trends, regardless of the underlying functional form. In contrast, linear regression aims to establish a predictive relationship by minimizing the sum of squared residuals (Bruce et al., 2020; Fávero et al., 2023). In this context, regression models based on e_{min} tend to produce better fits and higher coefficient of determination (R^2), which represents the proportion of the variation in the dependent variable that is explained by the regression model, indicating how well the data fit the proposed relationship.

Variations in material composition, such as varying fines content, may induce a simultaneous response in both linear CSL parameters, characterized by both vertical translation (governed by Γ_L) and rotation (governed by λ_e) in the e – log p' plane (Freire, 2022). Additionally, λ_e appears considerably more sensitive to void ratio measurement uncertainties than Γ_L, which may explain the larger data dispersion and weaker correlations frequently associated with λ_e in literature (Torres-Cruz, 2016), as can be seen by comparing the R^2 values in Figure 6a and Figure 6c.

The relationship between the linear CSL parameters is seldom addressed in literature, as these parameters are intrinsically linked from a physical standpoint. Nevertheless, Figure 7 illustrates this correlation: the considerable scatter indicates that the predicted values should be treated only as a rough reference to the measured data.

3.3.2 Non-linear CSL

The establishment of robust empirical relationships for non-linear CSL formulations remains challenging due to the intrinsic non-uniqueness associated with parameter calibration. Different combinations of fitting parameters may produce mathematically similar CSL envelopes, making the resulting coefficients strongly dependent on the adopted fitting methodology.

This limitation is clearly illustrated by the international round-robin testing program conducted by Reid et al. (2021). When evaluating the same material, different laboratories reported highly variable empirical fitting coefficients for non-linear CSL, while still obtaining comparable envelopes.

To address this limitation, all non-linear CSL parameters were recalculated in the present study for materials exhibiting non-linear behavior in the e – log p' plane. This procedure aims to improve methodological consistency and reduce variability associated with different fitting approaches reported in the literature.

Figure 8 presents the relationships between *FC* and the non-linear CSL parameters. Consistent with the trends identified in the Spearman's correlation matrix, *FC* exhibits only low to moderate correlations with parameters *b* and *c*. In contrast, parameter *a* does not show any significant correlation with fines content.

As indicated by the Spearman correlation matrix (Figure 2) and illustrated in Figure 9, minimum void ratio presents significant correlations with non-linear CSL parameters. Parameters *a, b* and *c* show a moderate linear relationship with e_{min}, when the influence of extreme values is reduced.

In contrast, weak or no significant correlations are observed with e_{max} for parameters *b* and *c*, either in the regression analysis or in the Spearman correlation matrix; only parameter *a* shows a significant correlation with e_{max} (see Figure 10).

As indicated by the Spearman correlation matrix, there is only one significant internal correlation among the non-linear CSL parameters (between *b* and *c*), as illustrated in Figure 11.

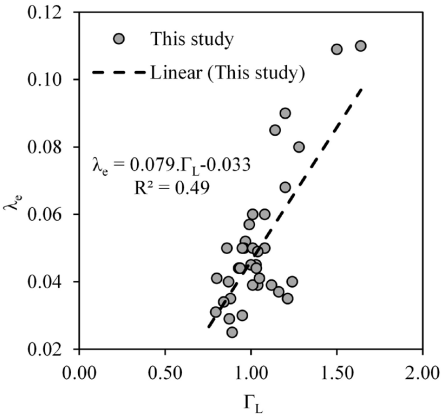


Figure 7. Correlation between linear CSL parameters Γ_L and λ_e.

As noted earlier, parameters *b* and *c* are linked to the same component of the non-linear CSL equation but given the highly significant relationship revealed by the Spearman correlation matrix, it seems more reasonable to employ parameter *c* as a predictor for parameter *b* in a regression analysis.

3.3.3 CSL instability and stability points correlations

A positive correlation is identified between G_s and the e_{inst} (Figure 12). This trend suggests that iron-rich tailings, characterized by higher G_s values, tend to reach instability at higher void ratios compared to silica-dominated tailings. This trend suggests that mineralogical density plays a secondary but non-negligible role in defining the geometric transition of the non-linear CSL.

A weak inverse relationship is observed between C_u and both the instability and stability void ratios (Figure 13). As C_u increases, materials tend to exhibit lower critical void ratios across the stress range, reflecting the improved packing efficiency of well-graded tailings. This behavior is consistent with the micromechanical principle that a wider range of particle sizes facilitates the infilling of interstitial voids, effectively shifting the CSL toward lower void ratio states.

Figure 14 highlights the relationship between e_{min} and the instability/stability transition points. Although inverse trends are observed between e_{min} and the instability/stability effective stresses (p'_{inst} and p'_{sta}), the correlations remain weak to moderate (R^2 of 0.20 and 0.39, respectively), suggesting that although packing density influences the stress level at which behavioral transitions occur, it is not the sole governing factor.

In contrast, the correlations between e_{min} and the void ratios at instability and stability (e_{inst} and e_{sta}) are positive, although still characterized by considerable scatter. This behavior indicates that the vertical positioning of the non-linear CSL is influenced by a complex interplay of factors beyond simple packing limits.

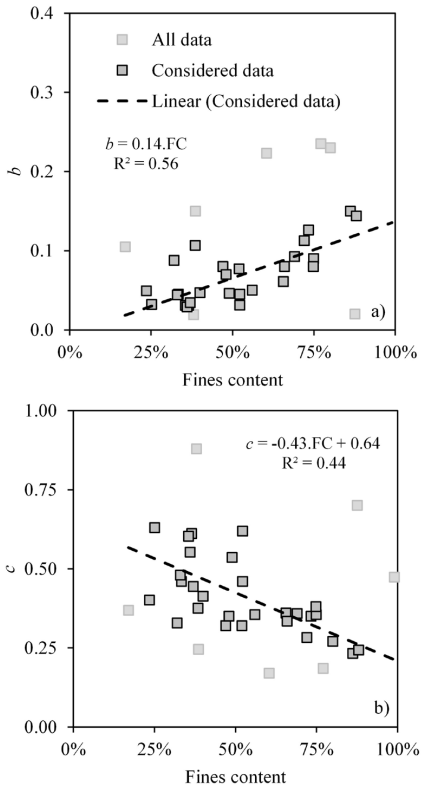


Figure 8. Correlation between fines content and non-linear CSL parameters a) *b* and b) *c*.

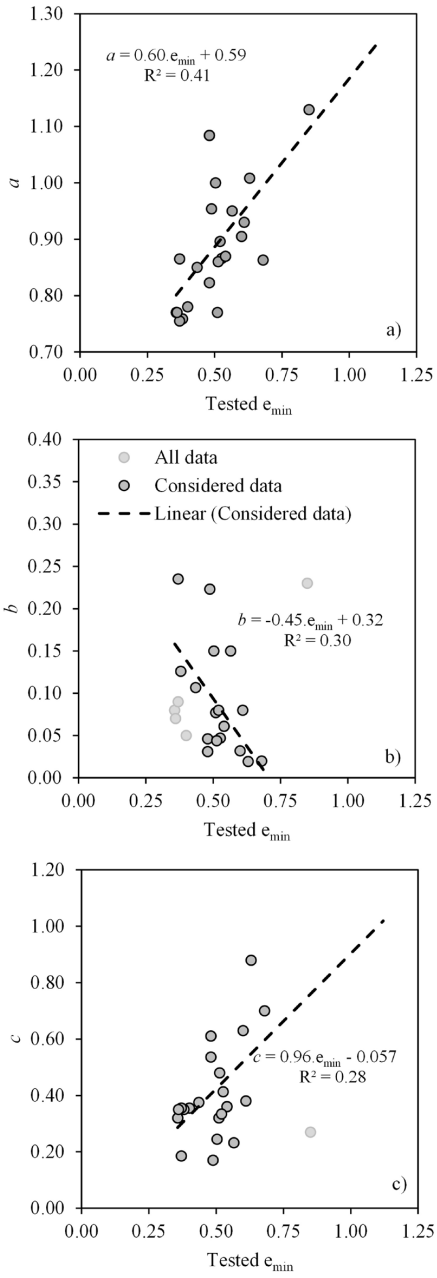


Figure 9. Correlation between minimum void ratio and non-linear CSL parameters a) *a*; b) *b*; and c) *c*.

CC BY

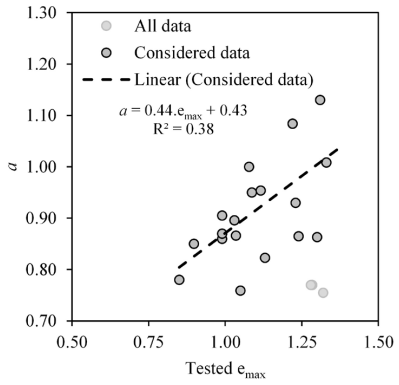


Figure 10. Correlation between maximum void ratio and non-linear CSL parameter *a*.

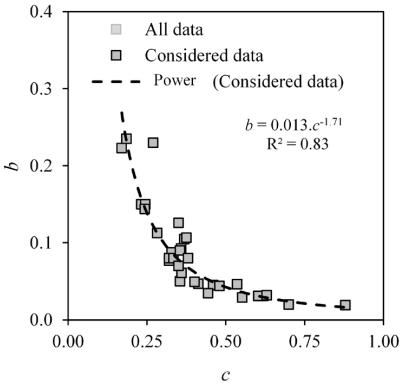


Figure 11. Correlation between non-linear CSL parameters *b* and *c*.

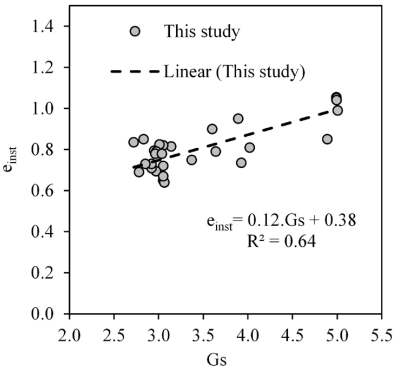


Figure 12. Correlation between instability void ratio and *Gs*.

In contrast to the trends observed for e_{min}, correlations involving the e_{max} and the instability/stability transition points are comparatively weaker and exhibit substantial scatter. This pronounced dispersion, likely reflecting the sensitivity of e_{max} to specimen preparation methods and inherent material heterogeneity (Li, 2017; Torres-Cruz & Santamarina, 2020), suggests that the loosest packing condition is less representative of the mechanisms governing these behavioral shifts. Ultimately, because critical transition states appear to be more strongly controlled by the densest achievable particle arrangement (Ccotohuanca & Klassen, 2024; Torres-Cruz & Santamarina, 2020), since the applicability of e_{max} as a reliable predictive parameter for CSL transitions is fundamentally limited.

Figure 15 illustrates the relationship between e_{inst} and the intercept parameters associated with both linear and non-linear CSL formulations. Positive correlations are observed in both cases, indicating that materials with higher CSL intercepts tend to exhibit instability at higher void ratios. The relationship is significantly stronger for parameter *a* (R^2 = 0.81). This result is expected, given that parameter *a* represents the low-stress intercept of the non-linear CSL and is therefore directly associated with the loose-state configuration. Since instability is concentrated in the low mean effective stress domain, the strong dependence between e_{inst} and *a* reinforces the importance of accurately capturing the low-stress curvature of the CSL.

Figure 16 explores the relationship of the e_{inst} with both the instability mean effective stress p'_{inst} and the stability void ratio e_{sta}. Regarding the stress conditions, a distinct threshold behavior is observed: within the void ratio interval of 0.6 to 0.8, lower values of e_{inst} correlate with markedly higher instability stresses p'_{inst}. However, as e_{inst} exceeds 0.8, this dependency diminishes, and the instability stress stabilizes within a narrower range of 50 to 150 kPa. Furthermore, the relationship between the void ratios suggests that the instability and stability transition states are intrinsically linked and evolve proportionally within the proposed framework. The near-linear proportionality indicates that materials exhibiting higher instability void ratios also tend to maintain higher void ratios at the stable transition state. This strong relationship suggests that the transition between instability and stable domains follows a systematic trajectory across different IOT. This behavior may indicate that both transition states are governed by the same underlying packing and compressibility mechanisms, despite occurring under distinct stress regimes.

3.4 Critical State Line parameters regressions

Guided by the Spearman correlation matrix and the bivariate relationships established in the preceding sections, Table 2 details the target parameters for the MLR analyses, along with their initial candidate predictors and the final predictors considered.

For the prediction of each parameter, a multiple linear regression model encompassing all potential predictors was initially established. A backward stepwise elimination method was then applied to iteratively discard non-significant variables. This procedure yielded a parsimonious final model, in which all remaining parameters were statistically significant at a 5% level ($p < 0.05$). The results and coefficients of these finalized models are presented in Table 3.

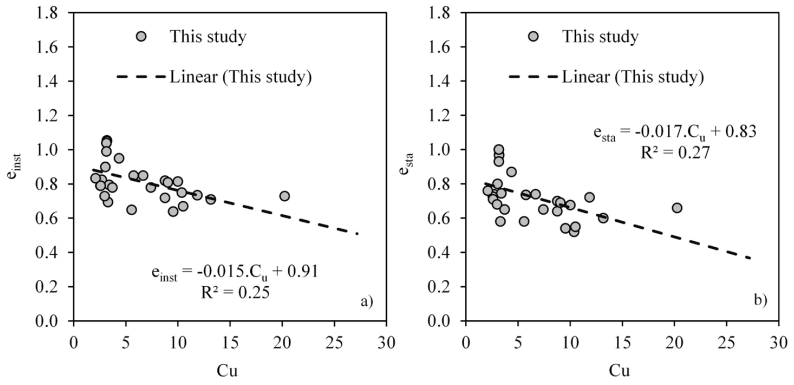


Figure 13. Correlation between a) e_{inst} and Cu and b) e_{sta} and Cu.

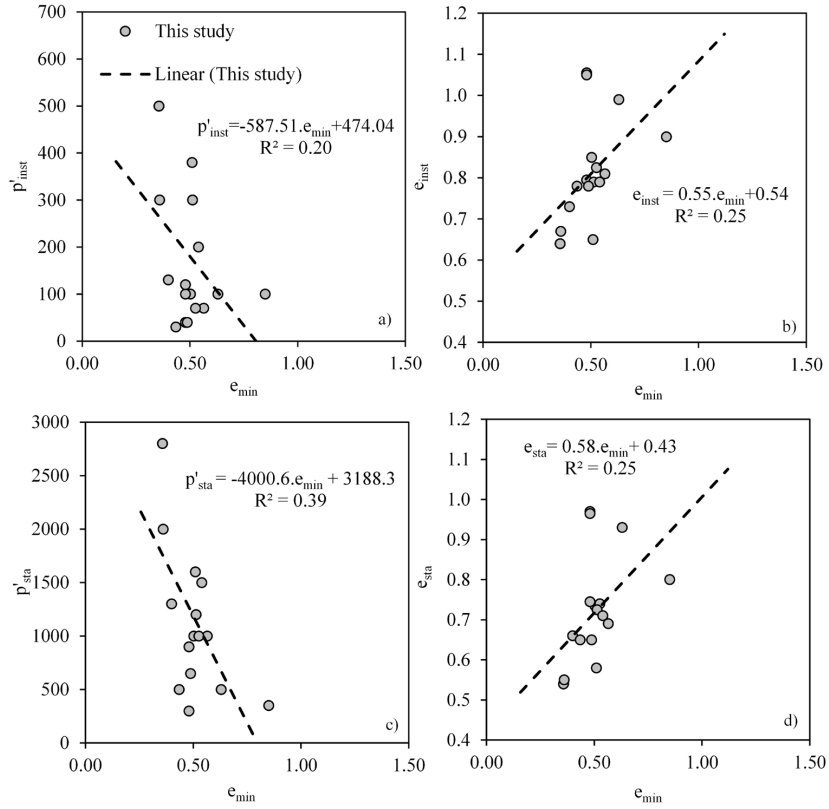


Figure 14. Correlation between minimum void ratio and a) p'_{inst}; b) e_{inst}; c) p'_{sta} and; d) e_{sta}.

Table 2. Parameters and predictors for multiple linear regression analysis.

Parameters	Initial predictors	Final predictor
Γ_L	e_{min}, e_{max}, G_s	e_{min}, G_s
λ_e	e_{min}, e_{max}, Cu	e_{min}
a	e_{min}, e_{max}, C_u, G_s	e_{min}, G_s
b	e_{min}, FC, C_u, G_s	c
c	e_{min}, FC, C_u, G_s	FC, G_s
e_{inst}	e_{min}, e_{max}, FC, C_u, G_s	e_{min}, FC, G_s
p'_{inst}	e_{min}, C_u, G_s	e_{min}

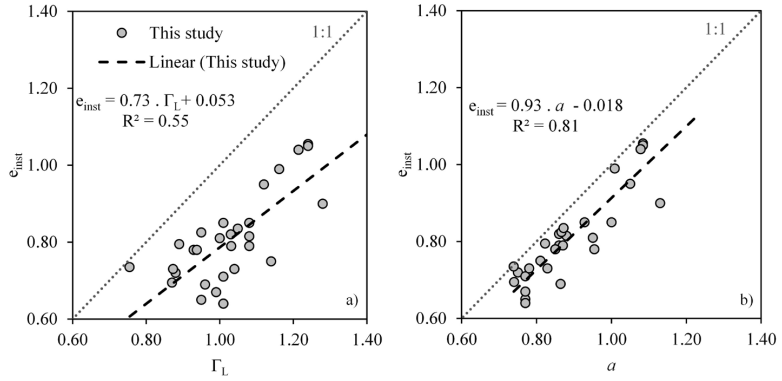


Figure 15. Correlation between instability void ratio and CSL parameters a) Γ_L and b) a.

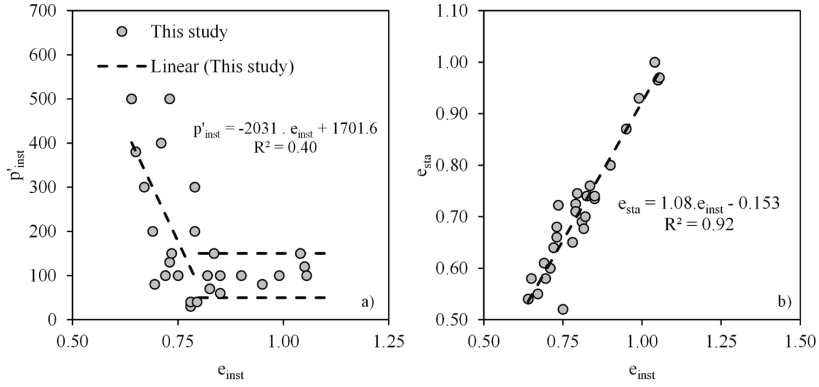


Figure 16. Correlation between instability void ratio and a) p'_{inst} and b) e_{sta}.

Table 3. Multiple linear regression models.

Parameter	β_0	β_1	X_1	β_2	X_2	β_3	X_3	Adjusted R^2	*RMSE*
Γ_L	0.3648	0.6870	e_{min}	0.0928	G_s	-	-	0.65	0.11
λ_e	0.0086	0.0762	e_{min}	-	-	-	-	0.48	0.02
a	0.4418	0.4449	e_{min}	0.0627	G_s	-	-	0.50	0.07
b	-	0.0126	$c^{-1.71}$	-	-	-	-	0.81	0.03
c	0.1927	-0.0022	FC	0.1044	G_s	-	-	0.35	0.12
e_{inst}	0.3377	0.4891	e_{min}	-0.0029	FC	0.1086	G_s	0.78	0.06
p'_{inst}	474	-588	e_{min}	-	-	-	-	0.15	140

Where β_0 is the model constant, β_i denote the regression coefficients, X_i represent the predictor variables of the model and *RMSE* is the Root Mean Square Error.

Parameter b exhibited no significant correlation with any of the initial predictive variables listed in Table 2. However, as evidenced by the Spearman correlation matrix and Figure 11, parameter b can be effectively described by a power-law relationship with parameter c. Consequently, to satisfy the linearity assumptions of the multiple linear regression analysis, a power transformation was applied to the predictor variable c.

Diagnostic checks confirmed the absence of autocorrelation and multicollinearity among the predictor variables across all models. Furthermore, the normality assumption for the residuals was satisfied for the majority of the models, with the exception of the predictive models for parameters c, yielding a Shapiro-Wilk test p-value of 0.04. To demonstrate the application of the proposed models, experimental data from three independent authors were compared against the predictions generated by the multiple linear regression models. This comparative analysis is illustrated in Figure 17, highlighting the specific predictor parameters employed by the models and real and estimated parameters.

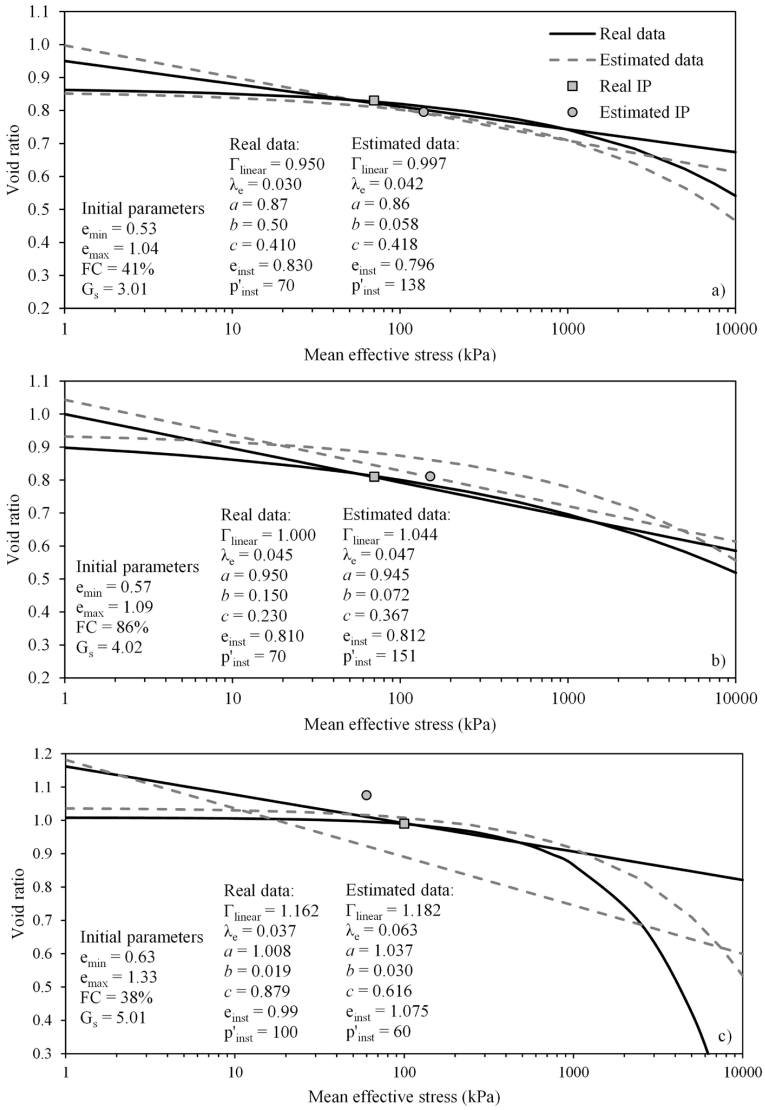


Figure 17. Comparison between real and estimated MLR data from a) Rios et al. (2025); b) Consoli et al. (2024c) and c) Cella & Padovani (2021).

The models demonstrated the best fit for the data in Figure 17a, where both the linear and non-linear CSLs closely approximated the experimental results. While the overall curvature and behavioral trends remain consistent across all three comparisons, the predicted lines in Figure 17b and Figure 17c exhibit a noticeable vertical translation relative to their experimental origin points. Despite this vertical shift, the general shape of the CSL is well captured by the model. Regarding the instability points, the void ratios show good agreement, with deviations falling within or close to the *RMSE* ranges detailed in Table 3.

It is imperative to note that, despite being statistically validated, these models rely on a limited dataset. They may serve as a preliminary tool for conceptual behavioral analysis, yet they should never replace actual laboratory tests for the definitive evaluation of real parameters.

4. Conclusion

Through a data-driven analysis of a global database, this study proposed a comprehensive framework to understand the critical state response of IOT, providing a practical, first-order screening tool for the preliminary assessment of their geomechanical behavior and stability domains.

The univariate assessment demonstrates that the compiled IOT exhibit pronounced physical and mineralogical heterogeneity; the dataset is statistically balanced and representative of real-world conditions. Retaining physical outliers and selecting core independent variables established a robust framework for the subsequent bivariate analyses.

Bivariate analysis reveals that *FC* is a limited predictor for critical state behavior. M is governed primarily by particle shape, and extreme void ratios show weak, scattered

CC BY

correlations with *FC*. Despite a conceptual "U-shaped" trend, pronounced data scatter confirms that packing efficiency and frictional strength do not depend solely on *FC*.

Micromechanically, *FC* marks structural transitions rather than directly predicting CSL behavior. Instead, e_{min} dictates material compressibility, governing both linear CSL parameters and the non-linear parameter *a*. Furthermore, mathematically, the non-linear CSL calibration suffers from non-uniqueness, as varying combinations of parameters *b* and *c* yield similar envelopes. Addressing this interdependence is crucial to reduce data scatter and establish reliable predictive models.

Transitions from flow instability to volumetric stability are intrinsically linked by a shared compressibility mechanism, evidenced by proportional void ratios. The densest packing state (e_{min}) reliably indicates these transitions, anchoring the material's behavior to the CSL's low-stress curvature, while properties like G_s exert only secondary controls.

In summary, MLR analysis provided a robust, first-order predictive framework for CSL parameters, successfully capturing complex interactions obscured by simple bivariate correlations. Validation against independent datasets confirms the framework's acceptable engineering accuracy for screening. However, while these data-constrained empirical models serve as a valuable screening tool for preliminary risk assessment, they cannot substitute advanced laboratory testing for site-specific geomechanical design.

Acknowledgements

The first and third authors acknowledge the Coordenação de Aperfeiçoamento de Pessoal de Nível Superior – Brasil (CAPES) for the scholarships granted. This study was financed in part by the Coordenação de Aperfeiçoamento de Pessoal de Nível Superior – Brasil (CAPES) – Finance Code 001. The second author acknowledges the Conselho Nacional de Desenvolvimento Científico e Tecnológico (CNPq) for the research productivity grant.

Declaration of interest

The authors have no conflicts of interest to declare. All co-authors have observed and affirmed the contents of the paper and there is no financial interest to report.

Authors' contributions

Leonardo Alberto do Nascimento: conceptualization, data curation, methodology, visualization, writing – original draft. Magnos Baroni: conceptualization, methodology, supervision, validation. Dêreck Hummel Becher: conceptualization, data curation, methodology, visualization, writing – original draft. Fernando Schnaid: conceptualization, supervision, validation, writing – review & editing.

Data availability

The datasets generated and analyzed in the course of the current study are available from the corresponding author upon request. Additionally, the database corresponding to Appendix A (Nascimento et al., 2026) is publicly available in the Zenodo repository at https://doi.org/10.5281/zenodo.20187285.

Declaration of use of generative artificial intelligence

This work was prepared with the assistance of generative artificial intelligence (GenAI) Gemini and NotebookLM with the aim of language polishing of the original text drafted by the authors, as well as to assist with Python scripting. The entire process of using this tool was supervised, reviewed and when necessary edited by the authors. The authors assume full responsibility for the content of the publication that involved the aid of GenAI.

List of symbols and abbreviations

a, b, c	Non-linear CSL fitting parameters
d	Diameter
e	Void ratio
e_c	Critical void ratio
e_{cs}	Void ratio at critical state
e_{cs0}	Normalized reference critical state void ratio (e_{cs} at 1 kPa)
e_{inst}	Instability void ratio
e_{max}	Maximum void ratio
e_{min}	Minimum void ratio
e_{sta}	Stability void ratio
p'	Mean effective stress
p'_{inst}	Mean effective stress at instability transition state
p'_{ref}	Reference mean effective stress
p'_{sta}	Mean effective stress at stability transition state
q	Deviatoric stress
C_c	Coefficient of curvature
CSL	Critical state line
CSSM	Critical state soil mechanics
C_u	Coefficient of uniformity
DSS	Direct simple shear
D_x	Particle diameter corresponding to x% passing in the particle size distribution curve
FC	Fines content
G_s	Specific gravity of solids
IOT	Iron ore tailings
M	Critical state stress ratio (q/p')
MLR	Multiple linear regression
M_{tc}	Critical state stress ratio at triaxial compression

PI	Plastic index
PSD	Particle size distribution
R^2	Coefficient of determination
$RMSE$	Root mean square error
TFC	Threshold fines content
WL	Liquid limit
WP	Plastic limit
β_0	Regression model intercept
β_i	Regression coefficients of the multiple linear regression model
λ_e	Slope of the linear critical state line in the $e - \log p'$ plane
v	Specific volume ($1 + e$)
σ_{3max}	Maximum effective confining stress
Γ_L	Intercept of the linear critical state line at p' = 1 kPa
Γ_{NL}	Intercept of the non-linear critical state line at p' = 1 kPa
Φ_{cs}	Critical state friction angle
X_i	Predictor variable in the multiple linear regression model
Ψ_{crit}	Critical state index defined as the difference between Γ_{NL} and e_{sta}

References

Almeida, M.S.S., Schnaid, F., Silva, R.S.A., Becker, L.D.B., Delgado, B.G., Souza Junior, A.J.P., Oliveira, F.W.A., Cavalcanti, M.C.R., & Nagula, S.S. (2025). Toward sustainable tailings disposal: a geotechnical overview of Brazilian research. *Soils and Rocks*, *48*(3), e2025011624. https://doi.org/10.28927/SR.2025.011624.

ASTM D4253. (2016a). *Standard Test Methods for Maximum Index Density and Unit Weight of Soils Using a Vibratory Table*. ASTM International, West Conshohocken, PA.

ASTM D4254. (2016b). *Standard Test Methods for Minimum Index Density and Unit Weight of Soils and Calculation of Relative Density*. ASTM International, West Conshohocken, PA.

ASTM D4318. (2017). *Test Methods for Liquid Limit, Plastic Limit, and Plasticity Index of Soils*. ASTM International, West Conshohocken, PA. https://doi.org/10.1520/D4318-17E01.

ASTM D7928. (2021). *Test Method for Particle-Size Distribution (Gradation) of Fine-Grained Soils Using the Sedimentation (Hydrometer) Analysis*. ASTM International, West Conshohocken, PA. https://doi.org/10.1520/D7928-21.

ASTM D854. (2023). *Test Methods for Specific Gravity of Soil Solids by Water Pycnometer*. ASTM International, West Conshohocken, PA. https://doi.org/10.1520/D0854-23.

Bedin, J. (2010). *Estudo do comportamento geomecânico de resíduos de mineração* [Doctoral thesis]. Universidade Federal do Rio Grande do Sul.

Bedin, J., Schnaid, F., Fonseca, A.V., & Costa Filho, L.M. (2012). Gold tailings liquefaction under critical state soil mechanics. *Geotechnique*, *62*(3), 263-267. https://doi.org/10.1680/geot.10.P.037.

Been, K., Jefferies, M.G., & Hachey, J. (1991). The critical state of sands. *Geotechnique*, *41*(3), 365-381. https://doi.org/10.1680/geot.1991.41.3.365.

Bouckovalas, G.D., Andrianopoulos, K.I., & Papadimitriou, A.G. (2003). A critical state interpretation for the cyclic liquefaction resistance of silty sands. *Soil Dynamics and Earthquake Engineering*, *23*(2), 115-125. https://doi.org/10.1016/S0267-7261(02)00156-2.

Bruce, P.C., Bruce, A., & Gedeck, P. (2020). *Practical statistics for data scientists : 50+ essential concepts using R and Python*. O'Reilly Media, Inc.

Carneiro, J.J.V. (2021). *Characterization and behaviour of iron ore tailings: the effect of compaction and stresses*. Universidade Federal de Viçosa.

Carrera, A., Coop, M., & Lancellotta, R. (2011). Influence of grading on the mechanical behaviour of Stava tailings. *Geotechnique*, *61*(11), 935-946. https://doi.org/10.1680/geot.9.P.009.

Carvalho, J.V. de A., Wagner, A.C., Scheuermann Filho, H.C., & Consoli, N.C. (2024). The role of fabric, stress history, mineralogy, and particle morphology on the triaxial behavior of nontextbook geomaterials. *Journal of Geotechnical and Geoenvironmental Engineering*, *150*(8), 04024055. https://doi.org/10.1061/JGGEFK.GTENG-12319.

Ccotohuanca, J., & Klassen, D. (2024). The critical state line parameters of iron ore tailings from basic laboratory tests: updated insights with additional data. *Proceedings of Tailings and Mine Waste*, *2024*, 379-391.

Cella, P.R.C., & Padovani, F.A. (2021). Five Brazilian tailings – from laboratory and field data towards safer design criteria. In *7th Internacional Conference Tailings Managment 2021*. Santiago: Gecamin.

Consoli, N.C., Azambuja Carvalho, J.V., Wagner, A.C., Scheuermann Filho, H.C., Carvalho, I., Cacciari, P.P., & de Sousa Silva, J.P. (2024a). Determination of critical state line (CSL) for silty-sandy iron ore tailings subjected to low-high confining pressures. *Journal of Rock Mechanics and Geotechnical Engineering*, *16*(5), 1684-1695. https://doi.org/10.1016/j.jrmge.2023.06.014.

Consoli, N.C., Scheuermann Filho, H.C., Wagner, A.C., Carvalho, J.V.A., Guedes, J.P.C., Carvalho, I., Delgado, B.G., & Silva, J.P.S. (2024b). Insights into the mechanics of uncemented and lightly cemented compacted iron ore tailings under high confining pressures. *Soil and Foundation*, *64*(6), 101543. https://doi.org/10.1016/j.sandf.2024.101543.

Consoli, N.C., Silva, J.P.S., Wagner, A.C., Carvalho, J.V.A., Baudet, B.A., Coop, M.R., Scheuermann Filho, H.C., Carvalho, I., Sousa, G.M., & Cacciari, P.P. (2024c). Critical state analysis of two compacted filtered iron ore tailings with different gradings and mineralogy at different stages of treatment. *Acta Geotechnica*, *19*(2), 881-898. https://doi.org/10.1007/s11440-023-01963-9.

Delgado, B.G., Fonseca, A.V., Bittar, R.J., Castilho, B. de M., & Coelho, D. (2023). Geomechanical behaviour of

CC BY

an iron ore tailings under high-stress levels for disposal by dry stacking. In *1st International Conference on Geotechnics of Tailings and Mine Waste* (pp. 342-351). London: ISSMGE.

Delgado, B.G., Viana da Fonseca, A., Bittar, R.J., Besenzon, D., Molina-Gómez, F., Cordeiro, D., Mendonça, A., & Rios, S. (2025). Critical state loci of superheavy iron ore tailings from sampling in brumadinho reservoir. *Journal of Geotechnical and Geoenvironmental Engineering*, *151*(10), 04025104. https://doi.org/10.1061/JGGEFK.GTENG-13055.

Fanni, R., Reid, D., & Fourie, A. (2024). Drained and undrained behaviour of a sandy silt gold tailings under general multiaxial conditions. *Geotechnique*, *75*(13), 195-214. https://doi.org/10.1680/jgeot.23.00186.

Fávero, L.P., Belfiore, P.P., & De Freitas Souza, R. (2023). *Data science, analytics and machine learning with R*. Academic Press. https://doi.org/10.1016/B978-0-12-824271-1.00034-2.

Fonseca, A.V. (2026). The 10th James K. Mitchell Lecture - In situ and lab tests work together to reduce uncertainties in TSF fragility assessment: a benchmark case-history. *Soils and Rocks*, *49*(2), e2026011425. https://doi.org/10.28927/SR.2026.011425.

Fonseca, A.V., Cordeiro, D., & Molina-Gómez, F. (2021). Recommended procedures to assess critical state locus from triaxial tests in cohesionless remoulded samples. *Geotechnics*, *1*(1), 95-127. https://doi.org/10.3390/geotechnics1010006.

Freire, A.S. (2022). *Influência do teor de finos no comportamento geomecânico de um rejeito de minério de ferro do Quadrilátero Ferrífero*. Universidade Federal de Ouro Preto.

Gonçalves, T.M., Pereira, F., Vizcarra, G.O.C., Coimbra, K.F., Wagner, A.C., Carvalho, J.V.A., Scheuermann Filho, H.C., & Consoli, N.C. (2025). Integrated field and laboratory framework for upstream tailings dam closure. *Indian Geotechnical Journal*. https://doi.org/10.1007/s40098-025-01441-x.

Hussien, M.N., & Sgaoula, J. (2023). Tailings state from basic laboratory tests and CPT data. In *Proceedings of Tailings and Mine Waste*, Vancouver, Canada. Fort Collins: Tailings & Mine Waste Conference.

Instituto Brasileiro de Mineração – IBRAM. (2025). *Relatório Anual de Atividades – 2024* (166 p.). IBRAM.

Jefferies, M., & Been, K. (2016). *Soil liquefaction: a critical state approach* (2nd ed.). CRC Press. https://doi.org/10.1201/b19114.

Ji, X., Xu, Q., Ren, K., Wei, L., & Wang, W. (2024). Critical state analysis for iron ore tailings with a fine-grained interlayer: effects of layering thickness and dip angle. *Water (Basel)*, *16*(20), 2958. https://doi.org/10.3390/w16202958.

Konrad, J.-M. (2001). Sand state from cone penetrometer tests: a framework considering grain crushing stress. *Geotechnique*, *51*(7), 651-652. https://doi.org/10.1680/geot.2001.51.7.651.

Lade, P.V. (1992). Static instability and liquefaction of loose fine sandy slopes. *Journal of Geotechnical Engineering*, *118*(1), 51-71. https://doi.org/10.1061/(ASCE)0733-9410(1992)118:1(51).

Lambe, T.W., & Whitman, R.V. (1979). *Soil mechanics*. John Wiley & Sons Inc.

Li, G. (2013). *Étude de l'influence de l'étalement granulometrique sur le comportement mecanique des materiaux granulaires* [PhD thesis]. Ecole Centrale de Nantes.

Li, W. (2017). *The mechanical behaviour of tailings*. City University of Hong Kong.

Li, W., & Coop, M.R. (2019). Mechanical behaviour of Panzhihua iron tailings. *Canadian Geotechnical Journal*, *56*(3), 420-435. https://doi.org/10.1139/cgj-2018-0032.

Macedo, J., & Petalas, A. (2019). Calibration of two plasticity models against the static and cyclic response of tailings materials. In *Tailings and Mine Waste Conference*. Fort Collins: Tailings & Mine Waste Conference.

Macedo, J., & Vergaray, L. (2022). Properties of mine tailings for static liquefaction assessment. *Canadian Geotechnical Journal*, *59*(5), 667-687. https://doi.org/10.1139/cgj-2020-0600.

Mitchell, J.K. (1976). *Fundamentals of soil behaviour*. John Wiley & Sons.

Mitchell, J.K., & Soga, K. (2005). *Fundamentals of soil behavior* (3rd ed). John Wiley & Sons Inc.

Morgenstern, N.R., Vick, S.G., Viotti, C.B., & Watts, B.D. (2016). *Report on the Immediate Causes of the Failure of the Fundão Dam*. Fundão Tailings Dam Review Panel.

Nascimento, L.A., Baroni, M., Becher, D.H., & Schnaid, F. (2026). A multivariable investigation of the critical state line in iron mine tailings - Appendix A [Dataset]. *Zenodo*. https://doi.org/10.5281/zenodo.20187285.

de Nóbrega, B.I.B. (2021). *Estados críticos em ensaios triaxiais em compressão e extensão e em cisalhamento simples num rejeito de minério de ferro*. Retrieved in May 18, 2026, from http://www.fe.up.pt

Oliveira, S.C. (2022). *Influência do Estado de Tensão na Obtenção dos Parâmetros de Estado Crítico de Rejeitos Filtrados de Minério de Ferro*. Universidade Federal de Ouro Preto.

Rabbi, A.T.M.Z., Rahman, M.M., & Cameron, D.A. (2019). The relation between the state indices and the characteristic features of undrained behaviour of silty sand. *Soil and Foundation*, *59*(4), 801-813. https://doi.org/10.1016/j.sandf.2019.05.001.

Reid, D. (2015). Estimating slope of critical state line from cone penetration test: an update. *Canadian Geotechnical Journal*, *52*(1), 46-57. https://doi.org/10.1139/cgj-2014-0068.

Reid, D., & Fanni, R. (2022). A comparison of intact and reconstituted samples of a silt tailings. *Geotechnique*, *72*(2), 176-188. https://doi.org/10.1680/jgeot.20.P.020.

Reid, D., Fanni, R., Koh, K., & Orea, I. (2018). Characterisation of a subaqueously deposited silt iron ore tailings.

Géotechnique Letters, *8*(4), 278-283. https://doi.org/10.1680/jgele.18.00105.

Reid, D., Fourie, A., Ayala, J.L., Dickinson, S., Ochoa-Cornejo, F., Fanni, R., Garfias, J., da Fonseca, A.V., Ghafghazi, M., Ovalle, C., Riemer, M., Rismanchian, A., Olivera, R., & Suazo, G. (2021). Results of a critical state line testing round robin programme. *Geotechnique*, *71*(7), 616-630. https://doi.org/10.1680/jgeot.19.P.373.

Rios, S., Viana da Fonseca, A., Caetano, I., Delgado, B., & Pereira, G. (2025). Comparison of geomechanical behavior of an iron ore tailings and natural siliceous silty sand with the same particle size distribution. *Canadian Geotechnical Journal*, *62*, 1-19. https://doi.org/10.1139/cgj-2025-0215.

Robertson, P. K., Melo, L., Williams, D. J., & Wilson, G. W. (2019). *Report of the Expert Panel on the Technical Causes of the Failure of Feijão Dam I*. Expert Panel Technical Report – PTEN.

Sadrekarimi, A. (2014). Static liquefaction-triggering analysis considering soil dilatancy. *Soil and Foundation*, *54*(5), 955-966. https://doi.org/10.1016/j.sandf.2014.09.009.

Salvatore, E., Modoni, G., Andò, E., Albano, M., & Viggiani, G. (2017). Determination of the critical state of granular materials with triaxial tests. *Soil and Foundation*, *57*(5), 733-744. https://doi.org/10.1016/j.sandf.2017.08.005.

Schnaid, F., Bedin, J., Viana da Fonseca, A.J.P., & de Moura Costa Filho, L. (2013). Stiffness and strength governing the static liquefaction of tailings. *Journal of Geotechnical and Geoenvironmental Engineering*, *139*(12), 2136-2144. https://doi.org/10.1061/(ASCE)GT.1943-5606.0000924.

Schofield, A., & Wroth, P. (1968). *Critical state soil mechanics*. McGraw-Hill.

Silva, J.P. de S., Cacciari, P.P., Torres, V.F.N., Ribeiro, L.F.M., & de Assis, A.P. (2022). Behavioural analysis of iron ore tailings through critical state soil mechanics. *Soils and Rocks*, *45*(2), 1-13. https://doi.org/10.28927/SR.2022.071921.

Silva, J.P.S., Rissoli, A.L.C., Cacciari, P.P., Viana da Fonseca, A.J.P., Scheuermann Filho, H.C., Wagner, A.C., Carvalho, J.V.A., Festugato, L., & Consoli, N.C. (2024). Triaxial testing response of compacted iron ore tailings considering a broad spectrum of confining pressures. *Soil and Foundation*, *64*(2), 101438. https://doi.org/10.1016/j.sandf.2024.101438.

Smith, K., Fanni, R., Chapman, P., & Reid, D. (2019). Critical state testing of tailings: comparison between various tailings and implications for design. *Proceedings of Tailings and Mine Waste*, *2019*, 1183-1195.

Thevanayagam, S., Shenthan, T., Mohan, S., & Liang, J. (2002). Undrained fragility of clean sands, silty sands, and sandy silts. *Journal of Geotechnical and Geoenvironmental Engineering*, *128*(10), 849-859. https://doi.org/10.1061/(ASCE)1090-0241(2002)128:10(849).

Torres-Cruz, L.A. (2016). *Use of the cone penetration test to assess the liquefaction potential of tailings storage facilities*. University of Witwatersrand.

Torres-Cruz, L.A., & Santamarina, J.C. (2020). The critical state line of nonplastic tailings. *Canadian Geotechnical Journal*, *57*(10), 1508-1517. https://doi.org/10.1139/cgj-2019-0019.

Verdugo, R., & Ishihara, K. (1996). The steady state of sandy soils. *Soil and Foundation*, *36*(2), 81-91. https://doi.org/10.3208/sandf.36.2_81.

Vick, S.G. (1990). *Planning, design and analysis of tailings dams* (2nd ed.). BiTech.

Wagner, A.C., de Sousa Silva, J.P., de Azambuja Carvalho, J.V., Cezar Rissoli, A.L., Cacciari, P.P., Chaves, H.M., Scheuermann Filho, H.C., & Consoli, N.C. (2023). Mechanical behavior of iron ore tailings under standard compression and extension triaxial stress paths. *Journal of Rock Mechanics and Geotechnical Engineering*, *15*(7), 1883-1894. https://doi.org/10.1016/j.jrmge.2022.11.013.

CC BY